Lecture 19

More on Hollow Waveguides

19.1 Rectangular Waveguides, Contd.

We have seen the mathematics for the TE modes of a rectangular waveguide. We shall study the TM modes and the modes of a circular waveguide in this lecture.

19.1.1 TM Modes (E Modes or $E_z \neq 0$ Modes)

The above exercise for TE modes can be repeated for the TM modes. The scalar wave function (or eigenfunction/eigenmode) for the TM modes, satisfying the homogeneous Dirichlet boundary condition on the entire waveguide wall is

$$\Psi_{es}(x,y) = A \sin\left(\frac{m\pi}{a}x\right) \sin\left(\frac{n\pi}{b}y\right) \tag{19.1.1}$$

Here, sine functions are chosen for the standing waves, and the chosen values of β_x and β_y ensure that the boundary condition is satisfied on the $x = a$ and $y = b$ walls. Neither of the m and n can be zero, lest the field is zero. Hence, both $m > 0$, and $n > 0$ are needed. Thus, the lowest TM mode is the TM_{11} mode. Notice here that the eigenvalue is

$$\beta_s^2 = \beta_x^2 + \beta_y^2 = \left(\frac{m\pi}{a}\right)^2 + \left(\frac{n\pi}{b}\right)^2 \tag{19.1.2}$$

which is the same as the TE case. Therefore, the corresponding cutoff frequencies and cutoff wavelengths for the TM_{mn} modes are the same as the TE_{mn} modes. Also, these TE and TM modes are degenerate. Furthermore, the lowest modes, TE_{11} and TM_{11} modes have the same cutoff frequency. Figure 19.1 shows the dispersion curves for different modes of a rectangular waveguide. Notice that the group velocities of all the modes are zero at cutoff, and then the group velocities approach that of the waveguide medium as frequency becomes large. These observations can be explained physically.

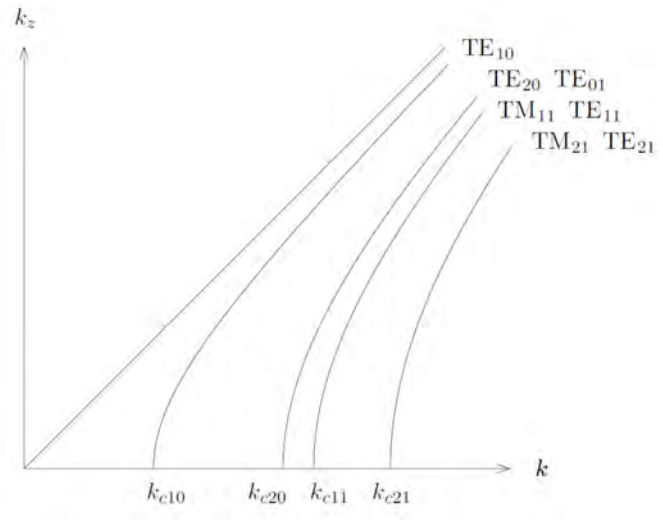

Figure 19.1: Dispersion curves for a rectangular waveguide. Notice that the lowest TM mode is the TM_{11} mode, and k is equivalent to β in this course (courtesy of J.A. Kong [31]). At cutoff, the guided mode does not propagate in the z direction, and the group velocity is zero. But when $\omega \to \infty$, the mode propagates in direction almost parallel to the axis of the waveguide, and hence, the group velocity approaches that of the waveguide medium.

19.1.2 Bouncing Wave Picture

We have seen that the transverse variation of a mode in a rectangular waveguide can be expanded in terms of sine and cosine functions which represent standing waves, or that they are

$$[\exp(-j\beta_x x) \pm \exp(j\beta_x x)]\,[\exp(-j\beta_y y) \pm \exp(j\beta_y y)]$$

When the above is expanded and together with the $\exp(-j\beta_z z)$ the mode propagating in the z direction, we see four waves bouncing around in the xy directions and propagating in the z direction. The picture of this bouncing wave can be depicted in Figure 19.2.

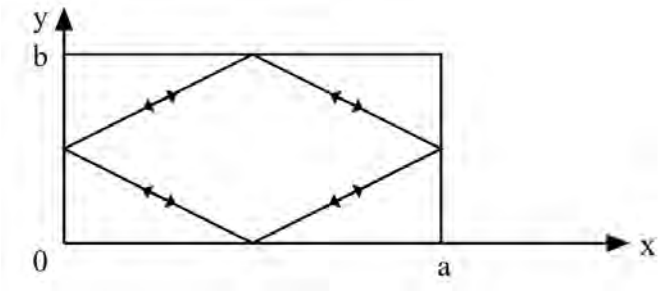

Figure 19.2: The waves in a rectangular waveguide can be thought of as bouncing waves off the four walls as they propagate in the z direction.

19.1.3 Field Plots

Given the knowledge of the scalar piloting potential of a waveguide, one can derive all the field components. For example, for the TE modes, if we know $\Psi_h(\mathbf{r})$, then

$$\mathbf{E} = \nabla \times \hat{z}\Psi_h(\mathbf{r}), \qquad \mathbf{H} = -\nabla \times \mathbf{E}/(j\omega\mu) \tag{19.1.3}$$

Then all the electromagnetic field of a waveguide mode can be found, and similarly for TM modes.

Plots of the fields of different rectangular waveguide modes are shown in Figure 19.3. Notice that for higher m's and n's, the transverse wavelengths are getting shorter, implying that β_x and β_y are getting larger because of the higher spatial frequencies involved. Higher frequencies are needed to make β_z real in order to propagate the higher order modes or the high m and n modes.

Notice also how the electric field and magnetic field curl around each other. Since $\nabla \times \mathbf{H} = j\omega\varepsilon\mathbf{E}$ and $\nabla \times \mathbf{E} = -j\omega\mu\mathbf{H}$, they do not curl around each other "immediately" but with a $\pi/2$ phase delay due to the $j\omega$ factor. Therefore, the $\mathbf{E}$ and $\mathbf{H}$ fields do not curl around each other at one location, but at a displaced location due to the $\pi/2$ phase difference. This is shown in Figure 19.4.

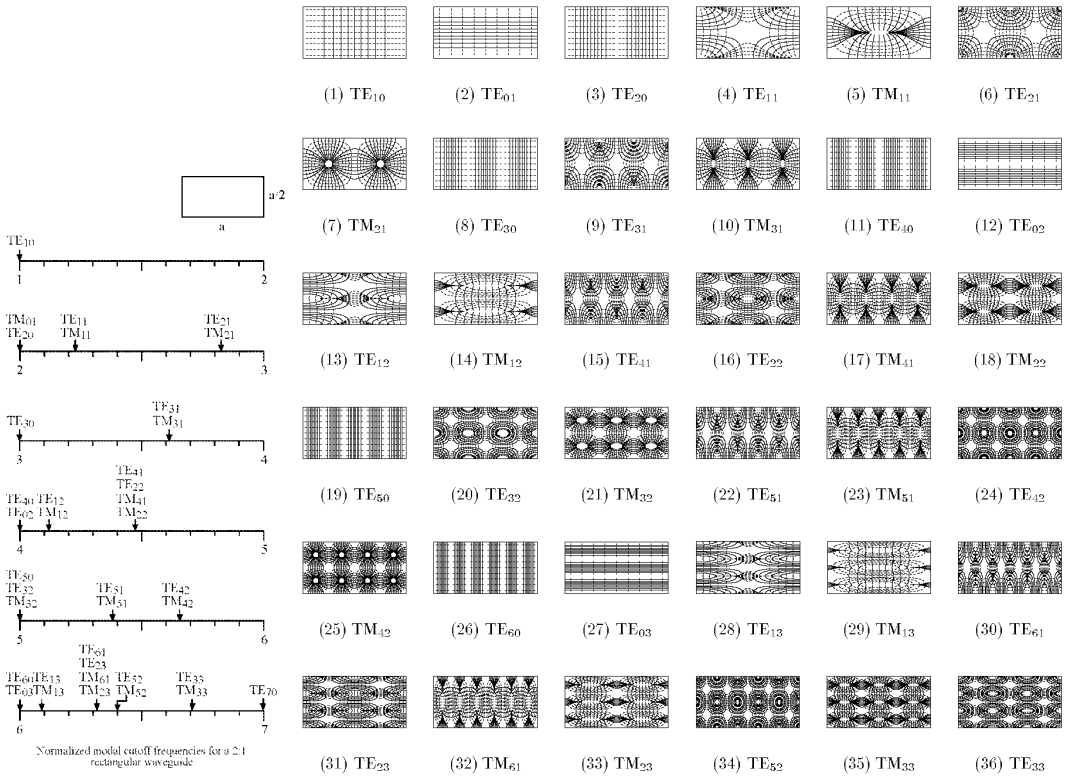

Figure 19.3: Transverse field plots of different modes in a rectangular waveguide (courtesy of Andy Greenwood. Original plots published in Lee, Lee, and Chuang, IEEE T-MTT, 33.3 (1985): pp. 271-274. [105]).

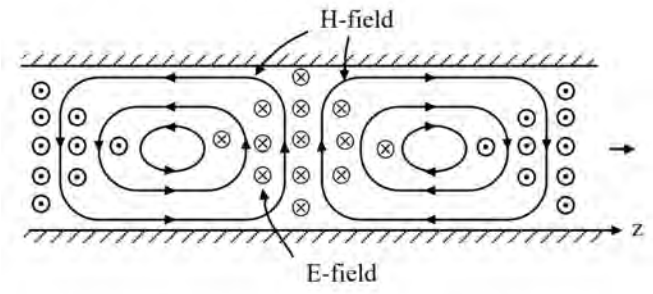

Figure 19.4: Field plot of a mode propagating in the z direction of a rectangular waveguide. Notice that the E and H fields do not exactly curl around each other.

19.2 Circular Waveguides

Another waveguide where closed-form solutions can be easily obtained is the circular hollow waveguide as shown in Figure 19.5.

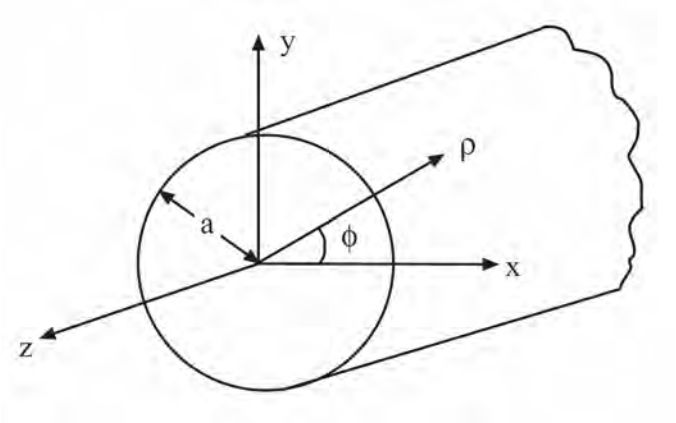

Figure 19.5: Schematic of a circular waveguide in cylindrical coordinates. It is one of the separable coordinate systems.

19.2.1 TE Case

For a circular waveguide, it is best first to express the Laplacian operator, ${\nabla_s}^2 = \nabla_s \cdot \nabla_s$, in cylindrical coordinates. Such formulas are given in [31, 106]. Doing a table lookup, $\nabla_s \Psi = \hat{\rho}\frac{\partial}{\partial \rho}\Psi + \hat{\phi}\frac{1}{\rho}\frac{\partial}{\partial \phi}$, $\nabla_s \cdot \mathbf{A} = \frac{1}{\rho}\frac{\partial}{\partial \rho}\rho A_\rho + \frac{1}{\rho}\frac{\partial}{\partial \phi}A_\phi$. Then

$$\left({\nabla_s}^2 + {\beta_s}^2\right)\Psi_{hs} = \left(\frac{1}{\rho}\frac{\partial}{\partial \rho}\rho\frac{\partial}{\partial \rho} + \frac{1}{\rho^2}\frac{\partial^2}{\partial \phi^2} + {\beta_s}^2\right)\Psi_{hs}(\rho, \phi) = 0 \tag{19.2.1}$$

The above is the partial differential equation for field in a circular waveguide. Using separation of variables, we let

$$\Psi_{hs}(\rho, \phi) = B_n(\beta_s \rho)e^{\pm jn\phi} \tag{19.2.2}$$

Then $\frac{\partial^2}{\partial \phi^2} \to -n^2$, and (19.2.1) simplifies to an ordinary differential equation which is

$$\left(\frac{1}{\rho}\frac{d}{d\rho}\rho\frac{d}{d\rho} - \frac{n^2}{\rho^2} + {\beta_s}^2\right)B_n(\beta_s \rho) = 0 \tag{19.2.3}$$

Here, we can let $\beta_s \rho$ in (19.2.2) and (19.2.3) be x. Then the above can be rewritten as

$$\left(\frac{1}{x}\frac{d}{dx}x\frac{d}{dx} - \frac{n^2}{x^2} + 1\right)B_n(x) = 0 \tag{19.2.4}$$

The above is known as the Bessel equation whose solutions are special functions denoted as $B_n(x)$.[1]

These special functions are $J_n(x)$, $N_n(x)$, $H_n^{(1)}(x)$, and $H_n^{(2)}(x)$ which are called Bessel, Neumann, Hankel function of the first kind, and Hankel function of the second kind, respectively, where n is the order, and x is the argument.[2] Since this is a second order ordinary differential equation, it has only two independent solutions. Therefore, two of the four commonly encountered solutions of Bessel equation are independent. Thus, they can be expressed then in term of each other. Their relationships are shown below:[3]

$$\text{Bessel,} \qquad J_n(x) = \frac{1}{2}[H_n{}^{(1)}(x) + H_n{}^{(2)}(x)] \tag{19.2.5}$$

$$\text{Neumann,} \qquad N_n(x) = \frac{1}{2j}[H_n{}^{(1)}(x) - H_n{}^{(2)}(x)] \tag{19.2.6}$$

$$\text{Hankel–First kind,} \qquad H_n{}^{(1)}(x) = J_n(x) + jN_n(x) \tag{19.2.7}$$

$$\text{Hankel–Second kind,} \qquad H_n{}^{(2)}(x) = J_n(x) - jN_n(x) \tag{19.2.8}$$

It can be shown that

$$H_n{}^{(1)}(x) \sim \sqrt{\frac{2}{\pi x}} e^{jx - j(n+\frac{1}{2})\frac{\pi}{2}}, \quad x \to \infty \tag{19.2.9}$$

$$H_n{}^{(2)}(x) \sim \sqrt{\frac{2}{\pi x}} e^{-jx + j(n+\frac{1}{2})\frac{\pi}{2}}, \quad x \to \infty \tag{19.2.10}$$

They correspond to traveling wave solutions when $x = \beta_s \rho \to \infty$. Since $J_n(x)$ and $N_n(x)$ are linear superpositions of these traveling wave solutions, they correspond to standing wave solutions. Moreover, $N_n(x)$, $H_n{}^{(1)}(x)$, and $H_n{}^{(2)}(x) \to \infty$ when $x \to 0$. Since the field has to be regular when $\rho \to 0$ at the center of the waveguide shown in Figure 19.5, the only viable solution for the hollow waveguide is that $B_n(\beta_s \rho) = AJ_n(\beta_s \rho)$. Thus for a circular hollow waveguide, the eigenfunction or mode is of the form

$$\Psi_{hs}(\rho, \phi) = AJ_n(\beta_s \rho) e^{\pm jn\phi} \tag{19.2.11}$$

To ensure that the eigenfunction and the eigenvalue are unique, boundary condition for the partial differential equation is needed. The homogeneous Neumann boundary condition on the PEC waveguide wall then translates to

$$\frac{d}{d\rho} J_n(\beta_s \rho) = 0, \quad \rho = a \tag{19.2.12}$$

Defining $J_n{}'(x) = \frac{d}{dx} J_n(x)$, the above is the same as

$$J_n{}'(\beta_s a) = 0 \tag{19.2.13}$$

[1] Studied by Friedrich Wilhelm Bessel, 1784-1846.

[2] Some textbooks use $Y_n(x)$ for Neumann functions.

[3] Their relations with each other are similar to those between $\exp(-jx)$, $\sin(x)$, and $\cos(x)$.

Plots of Bessel functions and their derivatives are shown in Figure 19.6. The above are the zeros of the derivative of Bessel function and they are tabulated in many textbooks. The m-th zero of ${J_n}'(x)$ is denoted to be β_{nm} in many books,[4] and some of them are also shown in Figure 19.7; and hence, the guidance condition for a waveguide mode is then

$$\beta_s = \beta_{nm}/a \tag{19.2.14}$$

for the TE_{nm} mode. From the above, β_s^2 can be obtained which is the eigenvalue of (19.2.1) and (19.2.3). It is a constant independent of frequency.

Using the fact that $\beta_z = \sqrt{\beta^2 - \beta_s^2}$, then β_z will become pure imaginary if β^2 is small enough so that $\beta^2 < \beta_s^2$ or $\beta < \beta_s$. From this, the corresponding cutoff frequency of the TE_{nm} mode is

$$\omega_{nm,c} = \frac{1}{\sqrt{\mu\varepsilon}} \frac{\beta_{nm}}{a} \tag{19.2.15}$$

When $\omega < \omega_{nm,c}$, the corresponding mode cannot propagate in the waveguide as β_z becomes pure imaginary. The corresponding cutoff wavelength is

$$\lambda_{nm,c} = \frac{2\pi}{\beta_{nm}} a \tag{19.2.16}$$

By the same token, when $\lambda > \lambda_{nm,c}$, the corresponding mode cannot be guided by the waveguide. It is not exactly precise to say this, but this gives us the heuristic notion that if wavelength or "size" of the wave or photon is too big, it cannot fit inside the waveguide.

19.2.2 TM Case

The corresponding partial differential equation and boundary value problem for this case is

$$\left(\frac{1}{\rho} \frac{\partial}{\partial \rho} \rho \frac{\partial}{\partial \rho} + \frac{1}{\rho^2} \frac{\partial^2}{\partial \phi^2} + {\beta_s}^2 \right) \Psi_{es}(\rho, \phi) = 0 \tag{19.2.17}$$

with the homogeneous Dirichlet boundary condition, $\Psi_{es}(a, \phi) = 0$, on the waveguide wall. The eigenfunction solution is

$$\Psi_{es}(\rho, \phi) = A J_n(\beta_s \rho) e^{\pm jn\phi} \tag{19.2.18}$$

with the boundary condition that $J_n(\beta_s a) = 0$. The zeros of $J_n(x)$ are labeled as α_{nm} is many textbooks, as well as in Figure 19.7; and hence, the guidance condition is that for the TM_{nm} mode is that

$$\beta_s = \frac{\alpha_{nm}}{a} \tag{19.2.19}$$

[4] Notably, Abramowitz and Stegun, Handbook of Mathematical Functions [107]. An online version is available at [108].

where the eigenvalue for (19.2.17) is β_s^2 which is a constant independent of frequency. With $\beta_z = \sqrt{\beta^2 - \beta_s^2}$, the corresponding cutoff frequency is

$$\omega_{nm,c} = \frac{1}{\sqrt{\mu\varepsilon}} \frac{\alpha_{nm}}{a} \tag{19.2.20}$$

or when $\omega < \omega_{nm,c}$, the mode cannot be guided. The cutoff wavelength is

$$\lambda_{nm,c} = \frac{2\pi}{\alpha_{nm}} a \tag{19.2.21}$$

with the notion that when $\lambda > \lambda_{nm,c}$, the mode cannot be guided.

It turns out that the lowest mode in a circular waveguide is the TE_{11} mode. It is actually a close cousin of the TE_{10} mode of a rectangular waveguide. This can be gathered by comparing their field plots: these modes morph into each other as we deform the shape of a rectangular waveguide into a circular waveguide. Figure 19.6 shows the plot of Bessel function $J_n(x)$ and its derivative $J_n'(x)$. Tables in Figure 19.7 show the roots of $J_n'(x)$ and $J_n(x)$ which are important for determining the cutoff frequencies of the TE and TM modes of circular waveguides.

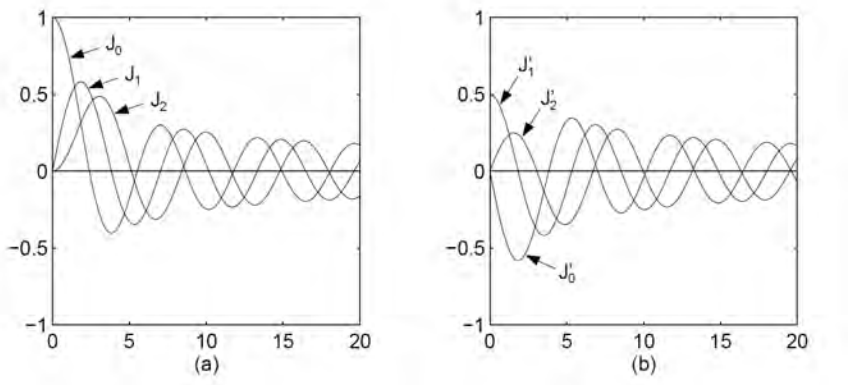

Figure 19.6: Plots of the Bessel function, $J_n(x)$, and its derivatives $J_n'(x)$. The zeros of these functions are used to find the eigenvalue β_s^2 of the problem, and hence, the guidance condition. The left figure is for TM modes, while the right figure is for TE modes. Here, $J_n'(x) = dJ_n(x)/dx$.

Table 2.3.1. Roots of $J_n'(x) = 0$.

n	β_{n1}	β_{n2}	β_{n3}	β_{n4}
0	3.832	7.016	10.174	13.324
1	1.841	5.331	8.536	11.706
2	3.054	6.706	9.970	13.170
3	4.201	8.015	11.346	14.586
4	5.318	9.282	12.682	15.964
5	6.416	10.520	13.987	17.313

Table 2.3.2. Roots of $J_n(x) = 0$.

n	α_{n1}	α_{n2}	α_{n3}	α_{n4}
0	2.405	5.520	8.654	11.792
1	3.832	7.016	10.174	13.324
2	5.135	8.417	11.620	14.796
3	6.380	9.761	13.015	16.223
4	7.588	11.065	14.373	17.616
5	8.771	12.339	15.700	18.980

Figure 19.7: Table 2.3.1 shows the zeros of $J_n'(x)$, which are useful for determining the guidance conditions of the TE_{mn} mode of a circular waveguide. On the other hand, Table 2.3.2 shows the zeros of $J_n(x)$, which are useful for determining the guidance conditions of the TM_{mn} mode of a circular waveguide.

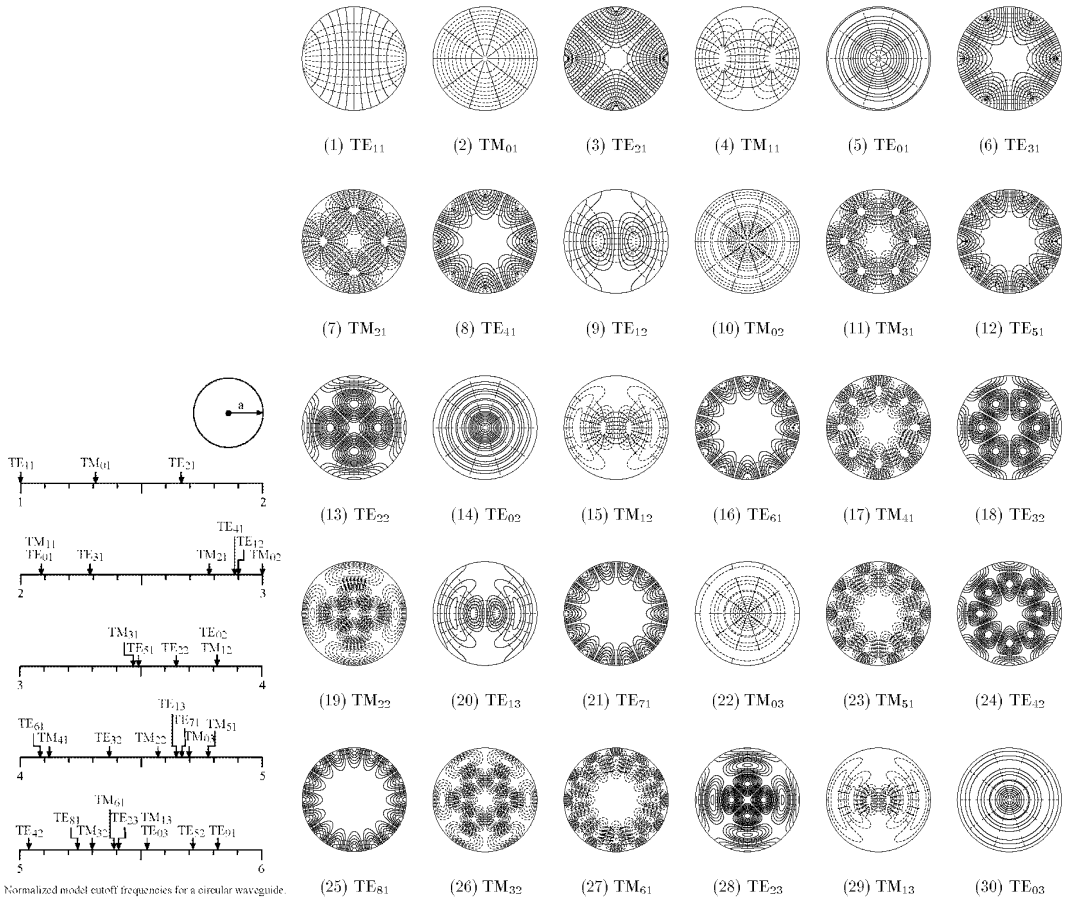

Figure 19.8: Transverse field plots of different modes in a circular waveguide (courtesy of Andy Greenwood. Original plots published in Lee, Lee, and Chuang [105]). The axially symmetric TE_{01} mode has the lowest loss, and finds a number of real-world applications.